Contribution To the Evaluation of Soot Deposit Thickness Evolution and Its Impact on Heat Transfer Within Heavy Diesel Engines: An Innovative Simplistic Procedure

A. Rahim [1], A. Beniaiche [2], L. Hemmouche [3], A. Liazid[*,4]
[1] Laboratory of Reactive Systems and Reaction, Ecole Militaire Polytechnique, Bordj El Bahri, Algiers; Algeria,
[2] Laboratory of Fluid Mechanics, Ecole Militaire Polytechnique, Bordj El Bahri, Algiers, Algeria,
[3] Materials Engineering Laboratory, Ecole Militaire Polytechnique, Bordj El Bahri, Algiers, Algeria,
[4] Sciences faculty, Physics department; University of Tlemcem, Algeria; Email: ab-liaz@hotmail.fr

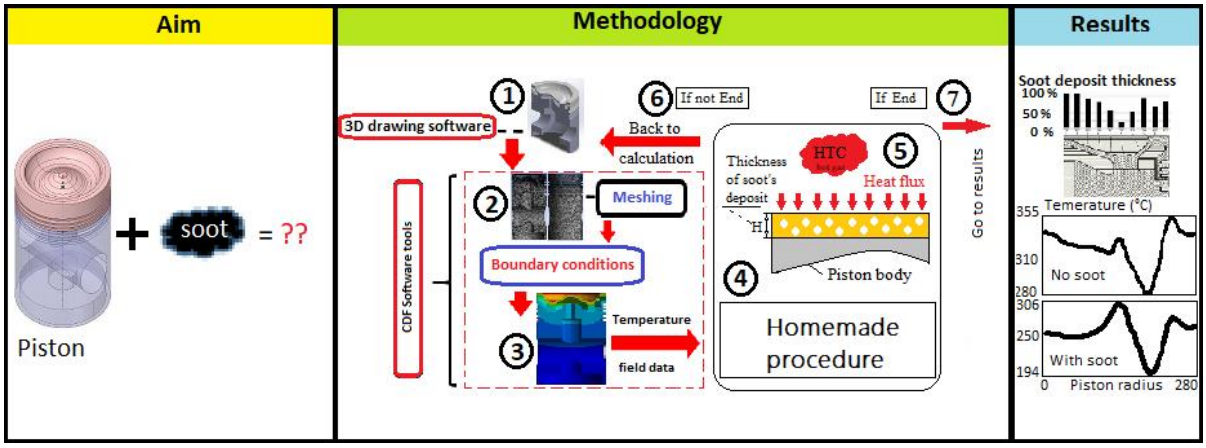

ABSTRACT: This study deals with a numerical procedure designed and built to evaluate the evolution of soot deposits thickness and their impact on heat transfer for a high-pressure common rail 16V280 marine diesel engine piston. Using a combination of 3D numerical computations and an iterative calculation algorithm, this work reveals the complex relationship between soot deposit, temperature distribution, and piston thermal dynamics. Non-uniform soot deposit distribution is observed, concentrated at the piston bowl peripheral regions. This distribution aligns with theoretical expectations, indicating the influence of the swirl effect. The presence of soot deposits alters the temperature distribution, implying displacement of high-temperature zones towards the bowl region of the piston. The reduction in surface temperature of approximately 14%, is attributed to the lower heat transfer coefficient of deposited layers. This greatly influences the distribution of thermo-mechanical stresses of the piston. The proposed procedure offers an approach to assess the impact of soot deposit on heat transfer. In addition, this study contributes to a better understanding of realistic piston conditions and addresses the challenges introduced by soot deposits in heavy-duty diesel engines by combining the proposed procedure with investigations based on CFD software tools.

الملخص: هذه الدراسة تتعامل مع الطريقة الرقمية تم تصميمها وبناؤها لتقييم تطور سمك الرواسب الكربونية وتأثيرها على نقل الحرارة لمحرك ديزل بحري ذو ضغط عالي من نوع 16V280 مزود بنظام الحقن المشترك. باستخدام مزيج من الحسابات العددية ثلاثية الأبعاد وخوارزمية حساب، تكشف هذه الدراسة عن العلاقة المعقدة بين رواسب الكربون، توزيع درجات الحرارة، وديناميات الحرارة للمكبس. يُلاحظ توزيعًا غير متجانس لرواسب الكربون، حيث تتركز في مناطق حافة الوعاء المكبسي. يتطابق هذا التوزيع مع التوقعات النظرية، مشيرًا إلى تأثير الدوران. تغير وجود رواسب الكربون توزيع درجات الحرارة، مما يشير إلى تحول مناطق درجات الحرارة العالية نحو منطقة الوعاء المكبسي. يُعزى تخفيض درجة حرارة السطح بنسبة تقريبًا 14% إلى انخفاض معامل نقل الحرارة للطبقات المتراكمة. وهذا يؤثر بشكل كبير على توزيع التوترات الحرارية الميكانيكية للمكبس. تقدم هذه الإجراءات المقترحة طريقة لتقييم تأثير رواسب الكربون على نقل الحرارة. بالإضافة إلى ذلك، تسهم هذه الدراسة في فهم أفضل لظروف المكبس الواقعية ومعالجة التحديات التي تطرحها رواسب الكربون في محركات الديزل للخدمة الشاقة باستخدام الخوارزمية المقترحة إضافة إلى أدوات برامج الديناميكية الحسابية للسوائل.

Keywords: Engine piston; piston modelling, soot deposit; piston stresses; piston temperature distribution.

الكلمات المفتاحية: مكبس المحرك، نمذجة المكبس، رواسب السخام، ضغوط المكبس، توزيع درجة حرارة المكبس.

Corresponding author's e-mail: ab-liaz@hotmail.fr

DOI:10.53540/tjer.vol.20iss2pp92-105

NOMENCLATURE

Abbreviations:

FEM	Finite Element Method
IC	Engine - Internal Combustion Engine
CCD	Carbonaceous Combustion Deposits
DI	Direct Injection
HCCI	Homogeneous Charge Compression Ignition
CFD	Computational Fluid Dynamics
kW	Kilowatts (unit of power)
mm	Millimeters (unit of length)
rpm	Revolutions Per Minute (unit of rotational speed)
MDO	Marine Diesel Oil
GPa	Gigapascal (unit of pressure or stress)
2D	Two-Dimensional
3D	Three-Dimensional
CFD	Computational Fluid Dynamics
NLPQL	Nonlinear Programming by Quadratic Lagrangian

Parameters:

A	Surface [m²]
A_i	Surface number i [m²]
A_s	Surface area involved in heat transfer [m²]
A_{ss}	Equivalent surface area for heat exchange of the solid part of the soot layer [m²]
As	Upper surface area of the soot layer [m²]
A_{ps}	Equivalent pore's surface area for heat exchange of pores [m²]
C_m	Constant
cp	Specific heat capacity [J/kg.K or J/g.K]
D_e	Hydraulic diameter [m]
D_c	Cylinder bore diameter [m]
H	Thickness of the soot deposit [m]
HTC_g	Heat transfer coefficient of the hot gases [W/m²K]
HTC_r	Heat transfer coefficient within the sub-regions positioned at r distance from the centre [W/m²K]
H_s	Thickness of the soot layer [m]
HTC	Heat Transfer Coefficient [W/m² °C]
HTC_i	HTC at the ith element [W/m² °C]
k	Thermal conductivity [W/m K]
k_p	Thermal conductivity of the pores [W/m K]
k_s	Thermal conductivity of the solid material (polycrystalline graphite) [W/m K]
k_{ST}	Effective thermal conductivity of the soot layer [W/m K]
m	Masse flow rate [m3/kg]
Nu	Nusselt number (a dimensionless number describing convective heat transfer)
P_g	Gas pressure (in Pa)
Pr	Prandtl number (a dimensionless number)
R	Radius of the piston's top area [m]
r	Radius [m]
R_c	Radius of curvature [mm]
Re	Reynolds number [-]
R_{hg}	Equivalent thermal resistance between hot gases and piston surface [m²•K/W]
R_p	Equivalent thermal resistance of pores [m²•K/W]
R_{ss}	Equivalent thermal resistance of the solid part of the soot layer [m²•K/W]
S	Surface area parameter [m²]
S_x	The surface area within the piston head [m²]
T	Temperature [°C of K]
T_{es}	Estimated temperature [°C of K]
T_g	Gas temperature [°C of K]
T_{hp}	Surface temperature of the piston head (°C or K)
T_{hg}	Temperature of the hot gases (°C or K)
T_m	Measured temperature [°C of K]
$T_{S.Ai}$ K].	Sub-surface temperature A_i [°C of
V_c	Volume of the combustion chamber [m³]
Vx	Velocity in the x-direction [m/s]

Greek Symbols:

φ	(HTC) Objective function used in the optimization procedure to assess the heat transfer coefficient (HTC) at each boundary element.
Φ	Crank angle [°]
μ	Dynamic viscosity of the fluid [Pa•s]
μ_m	Dynamic viscosity of the fluid at the bulk temperature [Pa•s]
ε	Material's porosity, a measure of the void fraction or open space within the material.
λ	Ratio of crank radius to connecting rod length [-]
ρ	Density [kg/m³]

Indexes:

c	Cylinder
g	Gas
hg	Hot gases
hp	Head of the piston
i	Element number i
m	Mean or measured
n	A variable representing the number of elements.
p	Pressure or piston
s	Solid
ss	Surface soot
soot	Soot
x	The x-direction

1. INTRODUCTION

The piston of the internal combustion engine creates the most stresses within the engine. The system operates under extreme thermal stress, lateral and axial loads, which can lead to serious damage from different types of applied forces. Therefore, designing a piston with high thermo-mechanical features is crucial to ensure its safe operation under different operating conditions. To achieve this goal, studying the thermo-mechanical loads is essential to prevent maximum failures. In recent years, the use of numerical investigations based on the finite element approach (FEM) in combination with semi-empirical correlations has become increasingly popular during the design process for various mechanical industries, especially those of the automotive industry and especially the internal combustion engines. Using such procedures allows engineers to evaluate the distribution of stress within the piston body, thereby improving the overall piston design.

CCD can induce diverse effects on engine performance. Pinto da Costa (2010) suggests that CCD might elevate the likelihood of engine knocking. Residual particles may heat up during combustion, potentially leading to self-ignition. Furthermore, CCD could diminish the heat transfer to the engine walls due to its insulating properties. This rise in surface temperature could generate hot spots, which may harbour reactive substances within the CCD structure, consequently promoting knocking combustion, Güralp (2008). In extreme scenarios, substantial deposits could even enhance knocking by effectively increasing the compression ratio.

Particularly in studies of DI engines using homogeneous charge and compression ignition, the thermal isolation provided by CCD becomes crucial. The insulation effect of the combustion chamber due to thermal isolation can bring about alterations in gas temperature and subsequently affect ignition timing, Güralp et al. (2009). The research work achieved by Hensel et al. (2009) demonstrated the necessity to modify conventional heat transfer models for HCCI engines since the peak heat flux arises at later crank angles compared to predictions from existing models. Work performed by Hoffman and Filipi (2015) highlighted that the limited operational range of low-temperature combustion is influenced by near-wall conditions. They studied the impact of CCD on thermal insulation, evaluating it using in situ thermocouples. Their results indicate that the crucial factor in the insulating effect is the porosity of the CCD rather than the fuel trapped in the pores. CCD might also facilitate the creation of fuel films on the piston. Drake et al. (2003) synthesized that smoke emissions likely originate from three main sources: (1) localized rich gas mixtures, (2) incompletely vaporized liquid fuel droplets, and (3) pool fires maintained by fuel films from the upper surface of the piston and other areas. The surface characteristics hold significance in terms of fuel-wall interaction and resultant fuel films. Distinctions arise when the fuel jet contacts a clean metal piston surface versus a porous deposit structure, which might behave like a sponge storing fuel. Kopple et al. (2014) examined the relationship between liquid fuel films, piston top temperatures, and soot deposits. Particularly during load transfers, they identified the interaction between the fuel spray and the piston surface as the main source of soot since the relatively low temperature at the top of the piston favours the formation of fuel film and its progressive combustion. Han et al. (2002) established a connection between the quantity of fuel within a piston surface film and the amount of resulting soot. Jiao and Reitz (2014) reinforced these conclusions by simulating spray-wall interaction and the soot formation process. Their study employed the Lagrangian particle approach outlined by O'Rourke and Amsden (1996, 2000). Near the wall regions, film vaporization altered the structure of turbulent boundary layers above the wall films due to the presence of gas velocities perpendicular to the wall caused by vaporization and the ensuing convective transfer of mass, momentum, and energy away from the film. The influence of the structure of the top piston surface should not be neglected. Desoutter et al. (2005) highlight that turbulent, chemically reactive multiphase flows within internal combustion engines are subject to the effects of combustion chamber walls. The presence of combustion chamber deposits (CCD) contributes to heat flux alterations, flow conditions, and reaction dynamics. Despite this, the specific mechanisms by which CCD formation modifies near-wall conditions remain unclear, even though they play a role in emission formation through shifts in turbulent momentum and heat transport. Utilizing synchrotron X-ray microtomography, Zhang et al. (2015) investigated the three-dimensional structures of carbon deposits on the piston surfaces of a large-scale, two-stroke marine diesel engine. Findings reveal a flat-bottomed piston carbon deposit (PCD) with irregular structures and uniform deposition. Tiny pores on the bottom surface suggest initial liquid film formation and nucleation boiling. PCD density decreases significantly below 150 μm thickness but remains constant from 150 to 1800 μm, indicating different formation mechanisms at these stages.

In their work, Weidenlener et al. (2018) delve into the intricate interplay between operating conditions and combustion chamber deposits (CCD) in internal combustion engines. Using advanced techniques, including optical profiling and energy-dispersive X-ray spectroscopy, they meticulously analyze CCD attributes such as surface structure, thickness, and thermal properties. Through direct numerical simulation and computational models, the researchers further illustrate CCD's impact on near-wall flow dynamics and heat transfer. This comprehensive exploration yields valuable insights into CCD behaviour, offering a deeper understanding of its implications for overall engine performance.

Although numerous experimental studies have explored heat transfer in combustion engines, only a limited number have investigated the influence of wall deposits in gasoline and diesel engines, as reported by Emi et al. (2002) and Kalghatgi et al. (1995). Numerical investigations of heat transfer have predominantly omitted the consideration of wall deposits, concentrating their focus exclusively on pristine surfaces, Noori et al. (2007) and Kubicki et al. (2007).

The central objective of this study is to scrutinize the influence of soot deposit effects using numerical investigations on heat transfer dynamics in a high-pressure 16V280 marine diesel engine piston. The authors endeavour to devise an easily implementable numerical methodology that is able to operate in conjunction with CFD codes. This approach is built to mitigate the intricate interdependencies among soot deposits, temperature distribution, and thermal dynamics. This methodology capitalizes on comprehensive perceptions of the internal temperature distribution of the piston and the encompassing boundary conditions.

2. RESEARCH CASE DATA

This work concerns the well-known high-pressure common rail 16V280 marine diesel engine. Table

01 gives its main parameters. The piston bowl is ω shape, and the piston material is 42CrMo. However, the piston skirt is LD11 alloy. Table 2 summarizes the important parameters of the materials composing the piston.

3. NUMERICAL METHODOLOGY

We used the SolidWorks® software to build the piston geometry and to transform it into finite elements, as illustrated in Figure 1 and Figure 2.

4. NUMERICAL MODEL

4.1 Grid domain

The mesh is refined at the top surface of the piston, the unloading groove, and the top surface of the piston inner cavity. The average mesh size is 1.6 mm. To improve the computing efficiency while maintaining accuracy, some simplifications are performed for the chamfering and rounding of the piston skirt and cavity below 3 mm. However, we conserved the original geometric features of the piston at its top surface without any simplification. The total number of computational grids for the piston is 381754, as illustrated in the figure 2.

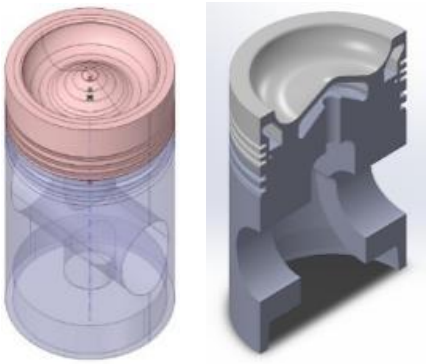

Figure 1: 3D view of the piston.

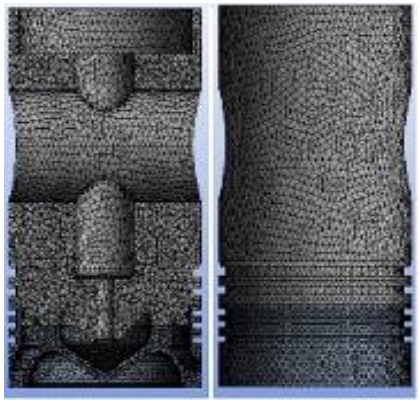

Figure 2: Piston geometry meshing. Inner and outside.

Table 1: Main parameters of 16V280 Diesel engine.

Parameter	Value
Number of cylinders	12
Cylinder bore	280 mm
Piston stroke	360 mm
Total displacement	95.4 liters
Compression ratio	13.5:1
Maximum power output	4920 kW
Maximum rotational speed	1000 rpm
Fuel type	Marine Diesel oil
Fuel injection system	943.18
Air system	Common-rail
	turbocharged and intercooler

Table 2: Materials properties of the piston**.**

Material properties	Value	
	Top	Top
Elastic modulus (GPa)	206	79
Poisson ratio	0.28	0.33
Thermal conductivity	40	138
Linear expansion coefficient (10-6/K)	12.1	20
Density (kg/m3)	7900	2800
Specific heat (J/kg°C)	460	880

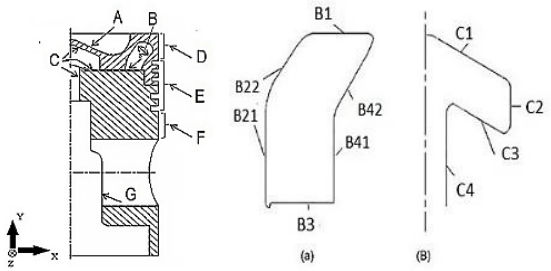

(Left) (Right)

Figure 3: Definition of the piston's seven zones**.**

4.2 Thermal Boundary Conditions

The thermal boundary conditions are essential for accurately studying the temperature field and the thermal load of the piston, and they are critical factors in determining the accurate solution. To resolve easily this issue, the piston geometry is decomposed into seven (07) zones, as depicted in Figure 3(left).

The main zones of the piston and their sub-zones are defined as follows:

A: The top surface of the piston is subdivided into ten (10) sub-zones.

B: The cooling gallery of the piton near the external side is subdivided into four (04) sub-zones, as depicted in Figure 3(right): B_Top=B1,B_outer=B41+B42,B_inner=B21 +B22 and B_bottom=B3.

C: The cooling gallery just under the piston bowl has a tube shape. This zone is decomposed into four sub-zones: C_inner=C4, C_top=C1, C_outter=C2, and C_bottom=C3.
D: The top external side of the piston is above the ring area.
E: The ring area is subdivided into twelve (12) sub-zones from top to bottom. They are named E1, E2 ,..., E11, E12;
F: The skirt of the piston.
G: The piston pin cavity.

Each zone has its proper initial boundary conditions, as summarized in Table 3.

After defining the new subdivisions of the piston geometry and calculating the initial values of temperature and HTC using the chosen semi-empirical correlations and/or previous experimental data provided by Liu et al. (2017), the next step is to modify these initial values for each region.

For the inverse heat conduction problem, the subdivision of the piston top region 'A' into n elements allows for an accurate assessment of the HTC at each one of those elements. An optimization procedure is then used to minimize an objective function φ(HTC), where the HTC is evaluated at the n boundary elements.

Find $\mathrm{HTC} \equiv \{\mathrm{HTC}_1, \ldots, \mathrm{HTC}_n\}$ minimizing $\varphi(HTC)$ Defined as:

$$\varphi(\mathrm{HTC}) \equiv \sum_{i=1}^{n}(\mathrm{T_m} - \mathrm{T_{es}})^2 \quad (13)$$

With T_{es} *and* T_m Are the estimated and the measured temperatures, and HTCi is the HTC at the i^{th} element.

Figure 4 illustrates the numerical process implementation. The fixed increment of 0.05% is imposed for difference calculations between the lower and upper boundary values. Convergence is set for 1% error.

For a steady-state temperature field, the medium temperature and heat transfer coefficient of the piston must be continuously adjusted for all regions until the required minimum relative error is achieved compared to the experimental results using NLPQL (Nonlinear Programming by Quadratic Lagrangian) gradient-based algorithm to provide a refined, local and optimized result. The final boundary conditions are presented in Table 4.

Table 3: Semi-empirical correlations used for each zone to define initial boundary conditions.

Zone	Correlation **(s)**
A	$HTC_g = 453.6\, Dc^{-0.214}\left(C_m P_g\right)^{0.786} T_g{}^{-0.525}$) (02) equations : $T_g = P_g\, V_x/(mR)$ (03) $V_x = V_c + \pi\, D^2\, S_x/4$ (04) $S_x =$ $S\left[1 - cos\,\varphi + \frac{1}{\lambda}\left(1 - \sqrt{1 - \lambda^2 sin^2\varphi}\right)\right]/2$ (05) Each region is evaluated using the following equations $A_1 = 2\pi \int_0^{0,1R} r\, dr.$ (06) For A2 to A10, the areas are calculated as follows: $A_i = \pi\,\{(i-1)^2 - (i)^2\}R^2$ (07) With: $i \in \{0.1,0.2,0.3,0.4,0.5,0.6,0.8,0.9,10\}$ and R is the radius of the piston head. The averaged HTC_mIt is defined at the head piston surface as: $HTC_m = \frac{1}{720}\int_0^{720} HTC_g\, d\theta.$ (08) For each one of the ten (10) sub-regions composing region A, HTC is evaluated as follows: $r < Rc, HTC_r =$ $\frac{2.2\, HTC_m}{\left(1+e^{0.1\left(\frac{Rc}{25.4}\right)^{1.9}}\right)} e^{0.1\left(\frac{Rc}{25.4}\right)^{1.9}}$ (09) $r > Rc, HTC_r = \frac{2.2\, HTC_m}{\left(1+e^{0.1\left(\frac{Rc}{25.4}\right)^{1.9}}\right)} e^{0.1\left(\frac{Rc}{25.4}\right)^{1.9}} +$ $0.05\, HTC_m\, [(r - Rc)/25.4]^{1.5/1.9}$ (10)
B	French Formula:
C	$Nu = 2.027(Re_B)^{0.466}(D_e/H)^{0.3}(Pr)^{0.33}$ $(\mu/\mu_m)^{0.14}$ (11)
D	HTC = 110 W/m²K, T = 650°C Liu et al. (2017)
E	Applying a planar multi-layer heat transfer assumption to the piston side, heat is transferred to the cooling water from the piston through its ring, which transmits it to the cooling oil inside the cavity and then to the cylinder envelope. (Liu et al. (2017))
G	$HTC = 5.3\,(B/2)(\Omega/60)(d_0/\vartheta_0)$ (12)

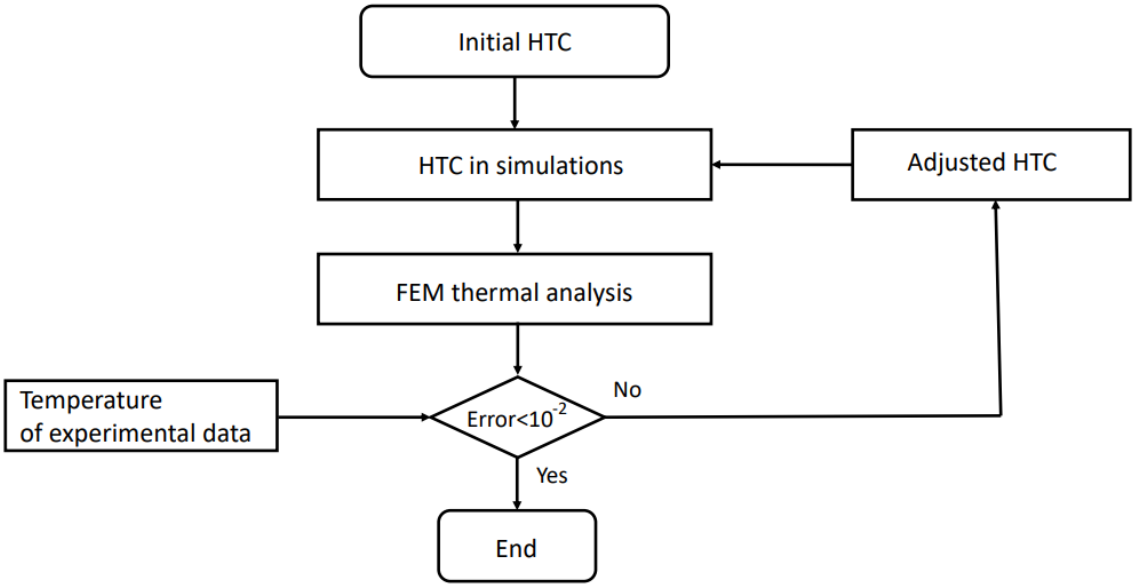

Figure 4: Procedure to evaluate the final boundary conditions.

Table 4: Initial and final boundary conditions.

	Initial values		Final values	
Zone	**HTC**	**T (°C)**	**HTC**	**T (°C)**
		A		
A1	550	750	550	710
A2	590	750	600	720
3	610	750	620	730
A4	640	750	650	740
A5	680	750	700	750
A6	830	750	910	850
A7	790	750	810	750
A8	560	750	550	730
A9	550	750	510	700
A10	540	750	500	700
		B		
B1	3000	110	2959,6	120
B2	320	110	300	120
B3	320	110	300	120
B4	320	110	300	120
		C:		
C1	1854	125	1851	135
C2	484	125	500	135
C3	2131	125	2123,34	135
C4	500	125	500	135
		D		
	120	650	110	650
		E		
E1	351	150	351	150
E2	64	180	70	200
E3	740	150	740	150
E4	461	150	461	120
E5	64	150	70	170
E6	742	150	742	120
E7	464	90	464	90
E8	68	130	70	140
E9	790	90	790	90
E10	150	260	150	260
E11	200	150	200	150
E12	200	180	200	180
		F zone		
	300	90	300	90
		G zone		
	3474	90	3000	90

5. SOOT DEPOSIT CHARACTERISTICS

5.1 Soot effective conductivity

The heat flux is calculated from the observed temperatures using both the inverse heat conduction equation and Duhamel's superposition equations. (Beck et al. (1985)).

In their computational and experimental investigation of deposits in Diesel engine cylinders, LaVigne et al. (1986) concluded that conduction is the predominant energy transmission-session mechanism in porous combustion systems.

$$k_{SOOT} = k_s.\left[(1-\varepsilon).1{,}5 + \varepsilon.0{,}25.\left(k_p/k_s\right)\right] \quad (13)$$

where k_p Is the conductivity of the pores, ε is the material's porosity, and k_{SOOT} It is the effective thermal conductivity of the soot layer. It is assumed that k_s Corresponds to the experimental values for polycrystalline graphite given by Pedraza and Klemens (1993). Szelagowski et al. (1999) state that conduction contributes most to the thermal conductivity of pores in the majority of applications.

5.2 Normal physical characteristics of soot's deposits

Table 5 lists the normal physical characteristics of soot as well as those of carbon and graphite.

Table 5: Physical properties of soot deposits, in comparison with carbon, graphite and diamond.

	Soot deposits	Carbon	Graphite
cp	840-1260	600-1000	708-717
k	0.07-1.6	1.7	119-168
ε		5-95%	
ρ	170-2180	1800-2100	1900-2300

6. SOOT MODELING ASSUMPTIONS

In the present study, we don't discuss the soot formation process. We built the following assumptions:
- Soot is supposed to be a porous media.
- Soot deposit is only formed at the head of the piston.
- The same final boundary conditions obtained for the clean piston are adjusted when considering the soot layers.
In the present study, soot is supposed to be composed of graphite.

6.1 Studied cases of soot deposit.

In the present study, two different cases of the piston are considered, denoted as Clean and Deposit cases. They are defined as follows:
• CLEAN CASE: This is the piston without any deposits, as shown in Figure 5a. The equivalent thermal resistance $R_{hot\ gases}$ between the hot gases at a temperature denoted T_{hg} and the outer surface of the piston body facing the hot gases denoted T_{hp} is calculated according to the equation (14):

$$R_{hg} = 1/(HTC_g.A_s) \quad (14)$$

With HTC_g Is the heat transfer coefficient of hot gases in [W/m²K] and A_s The surface of heat exchange between the piston body and hot gases in [m²]. HTC_g It is calculated using equation (15):

$$HTC_g = HTC_{conv.} + HTC_{rad.} \quad (15)$$

DEPOSIT CASE: In this case, the piston is supposed to be covered by a porous soot deposit, as illustrated in Figure 6a. The soot deposit is a porous layer with a thickness denoted H. The soot deposit has only one effective conductivity calculated using the equation (2). Figure 6b illustrates the equivalent thermal network.

Computations will be achieved using the equivalent thermal network. The added resistance, compared to the clean case, is the equivalent thermal resistance of pores R_p, and the one of the solid part of the soot layer denoted R_{ss}. They are calculated using equations (16) and (17):

$$R_p = 1/(HTC_g.A_{ps}) \quad (16)$$

$$R_{ss} = H_s/(k_s.A_{ss}) \quad (17)$$

With : HTC_g - The heat transfer coefficient within pores [W/ m²K] is equal to that of hot gases. A_{ps} - The equivalent surface of heat exchange of pores [m²], H_s- The thickness of the soot layer, k_s The conductive heat transfer coefficient of the solid part of the soot layer [W/m.K], A_{ss} The equivalent surface heat exchange of the solid part of the soot layer [m²].

6.2 Soot deposit assumptions

Determining the exclusive role of wall temperature effects in stabilizing deposit levels presents a significant challenge. Previous studies, such as those performed by Nakic et al. (1994), have firmly established that maintaining a minimum surface temperature around 310°C is necessary to prevent deposit formation. However, it is highly unlikely that the surfaces of the deposit layers can reach such elevated temperatures, even after subjecting them to a 40-hour testing period (which will be verified). Additionally, other crucial factors need consideration. This engine operates with a high residual content of approximately 45% and utilizes extremely lean air-to-fuel mixtures. When combined with the intensified combustion resulting from CCD formation, it becomes highly probable that deposit growth will be restricted at this specific operating point.
We present here a comprehensive procedure for evaluating the evolution of soot deposits on the top surface of a 3D piston geometry. The procedure uses the CFD code Fluent to simulate heat transfer and temperature distribution within the piston. It incorporates iterative steps to assess the presence and growth of soot deposits and accurately updates the boundary conditions. The procedure is based on logical assumptions and aims to provide an accurate understanding of soot deposits and their impact on heat transfer.

6.3 Procedure assumptions

We build the procedure on the following logical assumptions: (1) Soot deposits are considered homogeneous and time-independent in composition for simplicity. (2) Initial boundary conditions are specified, including heat transfer coefficients (HTC) and temperatures at various parts of the piston. (3) The presence of a soot deposit layer is identified when the temperature of a subregion falls below the threshold of 310°C. (4) The equivalent thermal resistance of the soot deposit is calculated by dividing the heat flux by the temperature gradient between the subregion and the top surface of the soot deposit, assumed to be equal to 310°C.

6.4 Procedure steps

We build the procedure on the following logical assumptions: (1) Soot deposits are considered homogeneous and time-independent in composition for simplicity. (2) Initial boundary conditions are specified, including heat transfer coefficients (HTC) and temperatures at various parts of the piston. (3) The presence of a soot deposit layer is identified when the temperature of a subregion falls below the threshold of 310°C. (4) The equivalent thermal resistance of the soot deposit is calculated by dividing the heat flux by the temperature gradient between the subregion and the top surface of the soot deposit, assumed to be equal to 310°C.

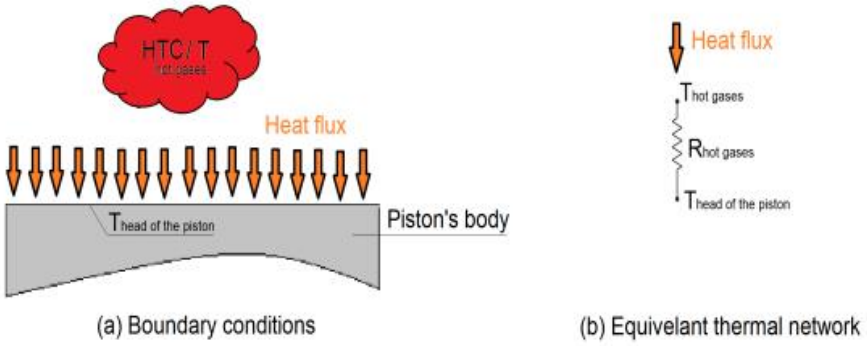

Figure 5: Schema of "Clean case": (a) Boundary conditions; (b) Equivalent thermal network

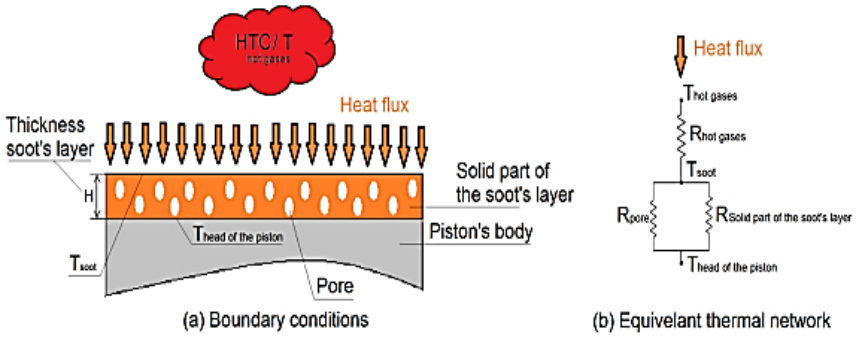

Figure 6: Schema of "Deposit case": (a) Boundary conditions; (b) Equivalent thermal network.

Figure 7 illustrates the diagram summarizing the procedure, providing a visual representation of the systematic process. This diagram serves as a useful reference for engineers and researchers seeking to implement the procedure in their investigations and design optimizations. We describe below the procedure steps:

Step (01): Define boundary conditions for HTC and T at each zone and proceed to step 02.

Step (02): Perform computations using CFD Fluent code and proceed to step 03.

Step (03): Obtain the heat flux map and the temperature distribution. Proceed to step 04.

Step (04): Check the temperature of each one of the ten (10) sub-surfaces in zone A. If all sub-surfaces have a temperature higher than 310°C, no soot layer is formed, and the procedure is terminated at step (18). If at least one sub-surface A_i If zone A has a temperature lower than 310°C, proceed to steps 05 and 06.

Step (05): For all sub-surfaces A_i with a temperature lower than 310°C, a soot layer is assumed to be formed at this sub-surface A_i . The upper surface temperature of this soot layer, on the gas side, is assumed to be equal to T_{ss} =310°C. This choice is based on the assumption that the height of the soot layer is currently unknown but is conditioned by the temperature of 310°C.

The equivalent thermal resistance $R_{1_{A_i}}$, for sub-surface A_i is given by equation (18):

$$R_{1_{A_i}} = \frac{1}{\frac{1}{HCT_{A_i}}} \quad (18)$$

with HCT_{A_i} is the equivalent thermal resistance occurring at the top area of the piston?

The soot layer has an equivalent thermal resistance given by the equation (19):

$$R_{2_{A_i}} = \frac{T_{ss} - T_{s.A_i}}{\phi_{A_i}} \quad (19)$$

with ϕ_{A_i} represents the heat flux at the sub-region A_i in [W/m²], T_{ss} is the temperature at the top area of the soot deposit assumed to be equal to 310°C and $T_{s.A_i}$ is the temperature of the sub-region A_i (obtained at step 03). The equivalent thermal resistance $R_{1_{A_i}}$ will have a new value for sub−surface A_i, given by the equation (20).

$$R_{1_{A_i}} = \frac{1}{\frac{1}{HCT_{A_i}} + R_{2_{A_i}}} \quad (20)$$

Step (06): Evaluate the average temperatures of sub-zones B1, B2, B3, B4, C1, C2, C3 and C4 using the results from step 03. Proceed to step 07.

Step (07): Determine the convective heat transfer coefficient at each one of the sub-surfaces: B1, B2, B3, B4, C1, C2, C3 and C4, using the French equation (21) to obtain the Nusselt number:

$$Nu = 2.027 (Re_B)^{0.466} (D_e/H)^{0.3} (Pr)^{0.33} (\mu/\mu_m)^{0.14} \quad (21)$$

with Re_B is the Reynolds number of the coolant fluid evaluated from the CFD code Fluent simulation. De/H is the ratio of the hydraulic diameter to the surface height. Pr is the Prandtl number of the coolant fluid and μ/μ_m is the dynamic viscosities ratio of the coolant fluid evaluated at the film temperature and the surface temperature, respectively. Proceed to step 08.

Step (08): The results from steps 05 and 07 are used as new boundary conditions to initiate numerical simulations with the CFD code Fluent. Proceed to step 09.

Step (09): Create a map of the heat flux distribution and temperature within the piston body. Proceed to step 10.

Step (10): Check if all the ten (10) sub-surfaces A_i have a temperature lower than 310°C. If all the ten (10) sub-surfaces have a temperature greater or equal than 310°C, the computation is complete. Proceed to step (18). If at least one surface A_i has a temperature under 310°C, proceed with steps 11 and 16 simultaneously as follows:

Step (11): Check if sub-surface A_i already has a soot layer. In the negative, proceed to step 12.

Step (12): For all sub-surfaces A_i without a soot layer, the temperature of the upper surface, on the gas side, is assumed to be equal to $T_{ss} = 310°C$. Hence, the soot layer has an equivalent thermal resistance $R_{1_{A_i}}$ given by the equation (9). Otherwise, the soot layer has an equivalent thermal resistance given by the equation (10). Including the convection term $\frac{1}{HCT_{A_i}}$, $R_{1_{A_i}}$ will have a new value for sub-surface A_i .Proceed to step 13.

Step (13): For all sub-surfaces A_i that already has a soot layer (condition from step 11), calculate the temperature of the hot gas side surface of the soot layer T_{ss}, using the heat flux ϕ_{A_i} , the temperature $T_{s.A_i}$, evaluated both in step 09 at A_i, and its equivalent thermal resistance $R_{2_{A_i}}$Evaluated at step 05, using equation (22). Proceed to step 14.

$$T_{ss} = T_{s.A_i} + \phi_{A_i} R_{2_{A_i}} \qquad (22)$$

Step (14): Check if the temperature of the external surface of the soot (hot gas side) T_{ss} is greater or equal to 310°C (for all sub-surfaces A_i that meets the condition of step 11). If "yes", proceed to step (18), end of the procedure. If "No", it is assumed that another layer of soot is formed on the top of the existing layer. Proceed to step 15.

Step (15): For all surfaces that meet the condition of step 14, a new layer of soot is supposed to be formed on top of the previous soot layer. The height of this new layer is unknown, but it is assumed that on the external surface of the new soot layer (on the hot gas side), the temperature is equal to 310°C. Calculate the equivalent thermal resistance. $R_{22_{A_i}}$of the new layer formed on the previous soot one, using equation (23):

$$R_{22_{A_i}} = \frac{310 - T_{s.A_i}}{\phi_{A_i}} \qquad (23)$$

where $T_{s.A_i}$ and ϕ_{A_i} are the temperature and heat flux at the sub-surface A_i (from step 09).

Calculate the equivalent thermal resistance of all soot layers (old and new) using equation (24):

$$R_{2_{A_i}} = R_{22_{A_i}} + R_{2_{A_i}} \qquad (24)$$

Finally, calculate the equivalent thermal resistance $R_{1_{A_i}}$ of sub-surface A_i, taking into consideration the convective term $(\frac{1}{HCT_{A_i}})$, using the equation (20).

Step (16): Evaluate the average temperatures of sub-zones B1, B2, B3, B4, C1, C2, C3, and C4 using the results from step 03. Proceed to step 17.

Step (17): Determine the convective heat transfer coefficient for each of the mentioned sub-surfaces B1, B2, B3, B4, C1, C2, C3, and C4, using the French equation to obtain the Nusselt number using equation (21).

The results from steps 10, 16, and 17 are used to define the new boundary conditions of the piston geometry, and the calculations loop back to step 08 until all external surfaces of the soot layer, facing hot gases, will have a temperature greater or equal than 310°C. Once this condition is met, the calculation stops at step (18) for the end of the procedure.

7. RESULTS AND DISCUSSIONS

7.1 Validation of the numerical model

It is crucial to verify the accuracy of the numerical results by comparing qualitative and quantitative temperature and heat flux distributions. The numerical results are validated by comparing them with experimental data from eight specific points within the piston geometry provided by Liu et al. (2017). Temperature contours within the piston body are plotted in figure 8, showing higher values at the top of the piston head and lower values towards the bottom cooling area. This trend was expected, as the hottest boundary conditions are located at the top of the piston due to the effect of hot gases, and the temperature decreases as heat is transferred to the cooling oil through the cooling cavities and water through the combustion chamber wall when approaching the cooling areas. The numerical temperature results are compared with experimental data at the same locations, as shown in Figure 8. The results indicate a very good concordance. The highest numerical temperature, 354.35°C, is observed at the bowl's edge, which matches well with the experimental measurement of 354°C at the same location. The other seven comparisons show good agreement with the experimental results. The maximum relative error of 3.90% is observed at point n°08.

Qualitatively, figure 8 shows the highest temperature values located at the piston bowl, while the lower values are found towards the bottom cooling area. This temperature field tendency is reasonable, considering that the hottest boundary conditions occur at the top of the piston due to the effect of hot gases.

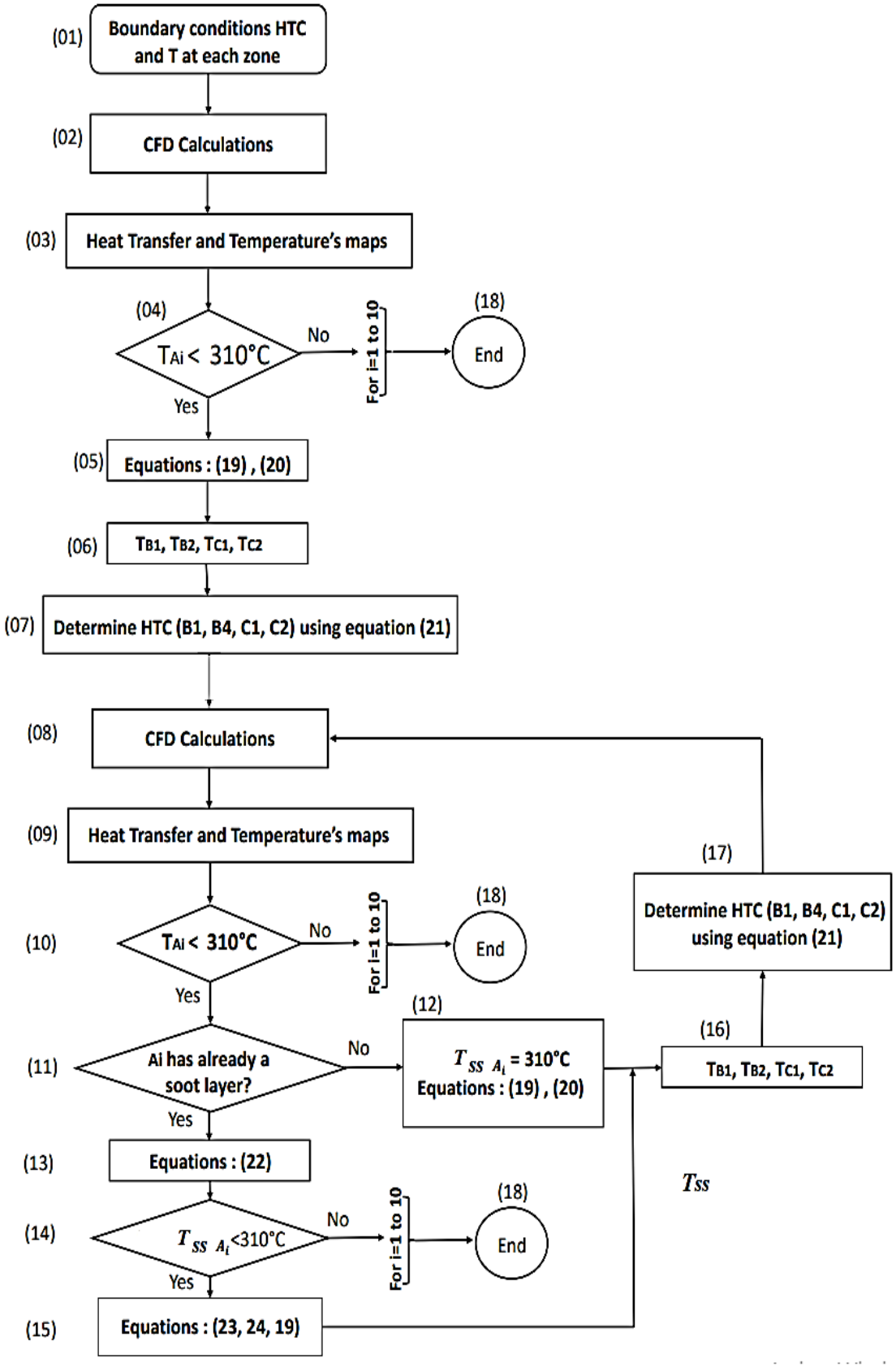

Figure 7: Illustration of the computing diagram procedure.

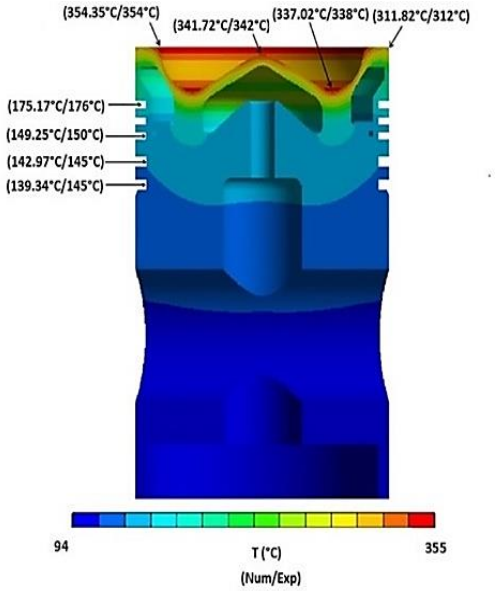

Figure 8: Temperature contours within the piston body; Numerical vs experimental data.

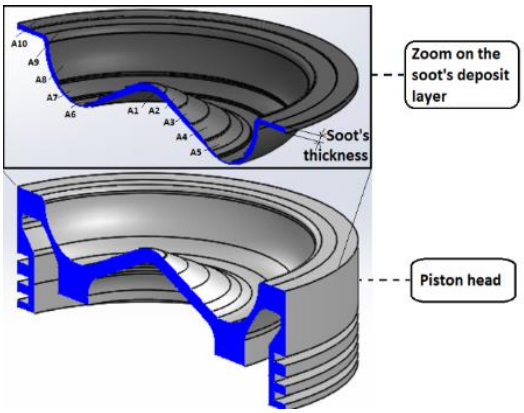

(a) Half 3D view

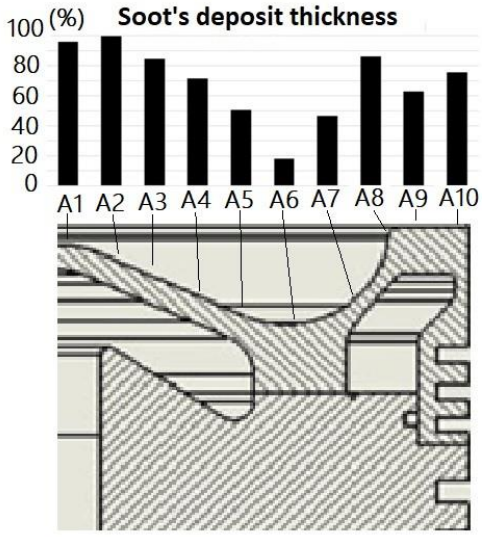

(b) Side view : Median plane

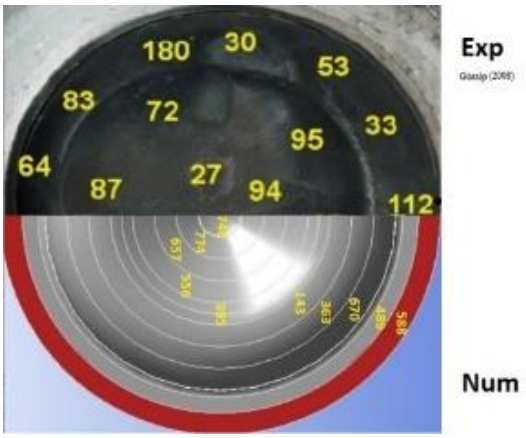

(c) Top view

Figure 9: Soot's deposit thickness: (a) Front view: Variation of the estimated soot's thickness (in %) over the zone A (b) Side view: Comparison of experimental and numerical data.

7.2 Soot deposit distribution results

Figures 9 (a and b) present half 3D view and the soot deposit distribution over the top area of the piston at its median plan, respectively. A subsequent to the completion of calculations. The data is presented in percentage of the highest recorded soot deposit thickness among the ten sub-regions "A1, A2,.....,A10". The absolute values of soot deposit thickness range between 0.143mm and 0.774 mm. As no experimental measurements are available for our case study or a closer case, we indicate for qualitative evaluation the experimental results provided by Güralp (2008) regarding a smaller GM MD-4 piston of an ignition engine (Bore: 86 mm, Stroke 94.6 mm, Compression Ratio 12.5:1). Figure 9(b) shows the top view comparing both experimental (Güralp (2008)) and present numerical data of the distribution of the soot deposit thickness (in micrometres), on the piston head surface. The experimental absolute values are located in the range of 0.027 mm to 0.180 mm. We note that the higher values appear on the peripheral side of the piston, similar to our results.

While we recognize the distinctions between our case and Güralp's study (2008), encompassing variations in piston geometry, fuel type, and engine operating conditions, we assert that our values are not exaggerated and seem reasonable considering the specific characteristics of the studied piston. Although direct experimental validation for our diesel engine case is currently unavailable, to the best of our knowledge, the data obtained still aligns with the range presented in Zhang et al.'s (2015) investigation. In their study, they employed synchrotron X-ray micro-tomography to non-invasively examine three-dimensional structures of carbon deposits on the surfaces of pistons within a large-scale two-stroke six-cylinder marine diesel engine (Model: 6S35ME-B9 MAN B&W, Bore & stroke (mm x mm): 350 x 1550). They reported that the thickness of soot deposits can reach values of up to 1800 µm.

7.3 Effect of soot's deposition on the surface temperature distribution

Figures 10. a and 10. b illustrate the temperature distribution across the symmetric plane at the upper region of zone A (beneath the layer of soot deposition). Obviously, the profile undergoes a notable transformation when a soot deposit occurs within zone A. Prior to the introduction of soot, the higher temperature value was located at the outer edge of the bowl. However, owing to the influence of the soot deposit, this elevated temperature diminishes and shifts towards the internal region of the bowl.

In the clean case, a peak temperature of 354.35°C appears at the bowl's edge within the upper piston region (0.125m < r < 0.130m), with 'r' denoting the piston radius. Conversely, with the soot deposit case, the maximum temperature of 306.92°C appears within the range of (0.075m < r < 0.080m).

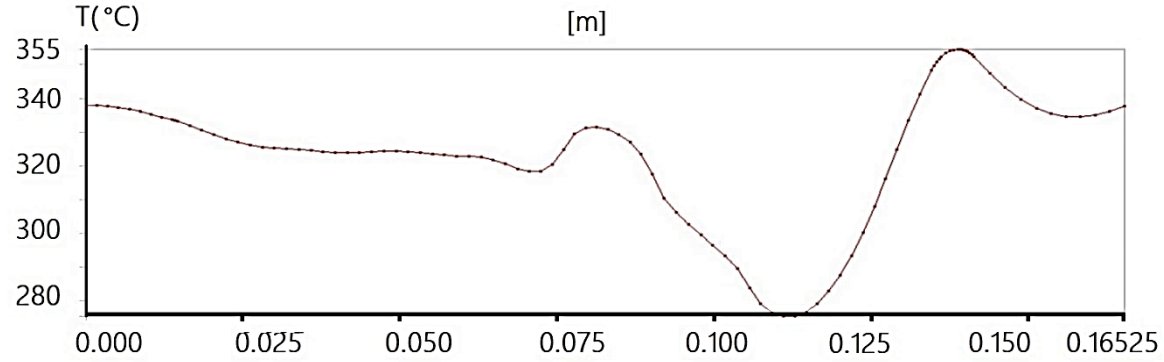

(a) Clean case

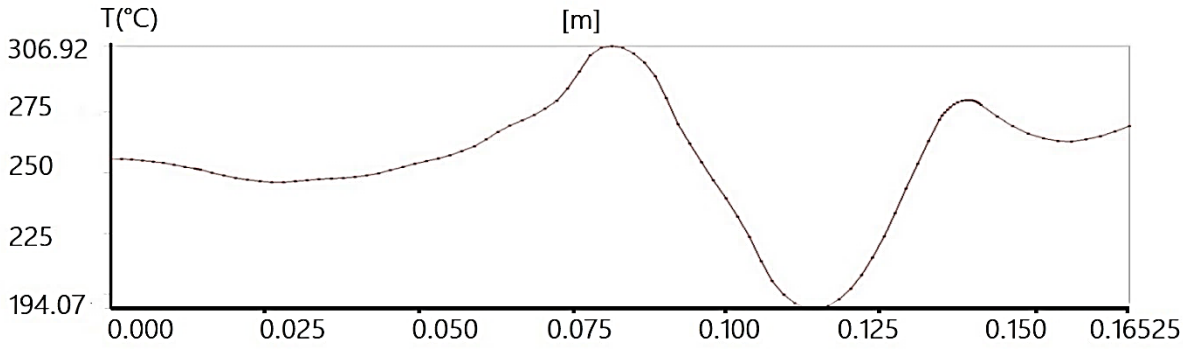

(b) Soot deposits

Figure 10: Temperature variation of the piston top surface: (a) Clean case; (b) Deposit case.

In addition, the lower temperature values exhibit quantitative changes but maintain their spatial position. In reality, the temperatures are around 275°C and 194.07°C for the clean and soot deposit cases, respectively. These values are located in the

range of (0.110 m < r < 0.120 m). The observed variation in the temperature curve along the piston radius at the upper region can be attributed to the variance in soot deposit thickness, as depicted in figure 10a. This plot elucidates the fluctuations in soot thickness across the ten sub-regions constituting zone A, expressed as a percentage of the maximum estimated soot deposit thickness.

Significantly, the presence of soot deposits not only reduces the surface temperature but also influences its spatial distribution. This, in turn, holds implications for the internal heat transfer processes within the piston body. To validate this hypothesis, Figure 11 shows the temperature variation across the piston body for the clean case, figure 11. a, and the deposit case Figure 11. b, respectively.

Figure 11 underscores the substantial influence of soot deposit on the temperature distribution within the piston body. While the upper portions of the piston area (top and skirt) continue to exhibit the highest temperature values, a marked departure from uniform temperature distribution becomes evident, particularly within the central bowl region, as compared to the clean case.

Intriguingly, the elevated temperature values of the deposit case are concentrated at a localized area of the bottom of the bowl. This contrasts with the uniform distribution observed in the clean case. Notably, the positions of maximum

temperature values have shifted towards this specific area, departing from their previous location at the external edge of the bowl.

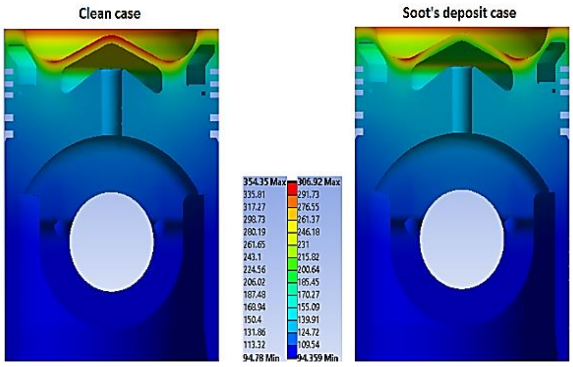

Figure 11: Temperature distribution over the piston body: (a) Clean case, (b) deposited case.

On the upper surface of the metal or under the soot deposit layer, the temperature decrease is due to deposit application, characterized by its relatively lower heat transfer coefficient. Deposit induces a temperature reduction on the metal surface (14% lower than the clean piston surface) for an identical piston configuration.

The present procedure offers several advantages for evaluating soot deposits on 3D piston geometries. Firstly, it ensures accuracy by validating heat transfer calculations against experimental data, establishing the reliability of the results. Secondly, the iterative approach implemented in the procedure allows for the realistic simulation of soot deposit growth and behaviour, providing a detailed understanding of their effects on heat transfer. This enables engineers to gain valuable insights into optimizing combustion systems and minimizing deposit-related issues. Furthermore, the procedure is flexible and compatible with existing engineering practices, making it applicable to real-world scenarios. It can be seamlessly integrated into the design and analysis processes, facilitating a comprehensive analysis of soot deposits. By considering the interaction between soot deposit and heat transfer, the procedure assists in optimizing heat transfer efficiency and enhancing the overall performance of combustion systems.

8. CONCLUSION

This research presents a comprehensive exploration of the intricate interplay between soot deposition and heat transfer in a high-pressure common rail 16V280 marine diesel engine piston. Our meticulously designed methodology has provided critical insights into the effects of soot deposits on temperature distribution, thermal dynamics, and overall piston behaviour.

The study uncovers a non-uniform distribution of soot deposits across Zone A, concentrating thicker deposits in the bowl and peripheral regions. This non-uniformity significantly alters the thermal dynamics, redistributing thermal stress across various surfaces and valves within the combustion chamber.

Analyzing temperature distribution reveals the profound impact of soot deposits on piston thermal behaviour, particularly in the localized area at the bottom of the bowl, where elevated temperature values concentrate due to the influence of soot deposits. This localized deviation from the previously observed uniform temperature profile is a critical finding with implications for engine efficiency and durability.

Moreover, the investigation highlights the influence of soot deposits on surface temperatures, resulting in a temperature decrease on the metal surface or under the soot deposit layer. This reduction, approximately 14% lower than the clean piston surface under identical piston configurations, underscores the importance of considering soot deposits in engine design and optimization.

In light of these findings, we propose the following recommendations for future research and practical applications:

- Optimizing Operating Conditions: Explore engine tuning and combustion optimization strategies to minimize the concentration of soot deposits, promoting a more uniform distribution.
- Adapting Design Parameters: Focus on modifications to future designs that account for altered temperature profiles induced by soot deposits. This may include adjustments to piston geometry, surface treatments, or innovative cooling mechanisms.
- Heat Transfer Enhancement Techniques: Investigate advanced coatings or materials with improved heat transfer properties to compensate for the lower heat transfer coefficients associated with deposited layers. Explore alternative cooling methods for critical engine components.
- Validation of Numerical Models: The numerical methodology presented in this study, incorporating 3D numerical investigations and iterative computing, serves as a powerful tool. However, further validation and refinement of these numerical models are recommended. Experimental validation using real-world engine data can enhance the accuracy and reliability of the numerical simulations, providing more confidence in the insights obtained.

These recommendations aim to enhance the practical application of our findings, providing actionable insights for optimizing internal combustion engines under realistic operating conditions. By incorporating these considerations, we contribute to the broader applicability of our study's outcomes and advance engine technology towards increased efficiency and sustainability.

CONFLICT OF INTEREST

The authors declare that there are no conflicts of interest regarding this article.

FUNDING

The research underpinning this publication was undertaken independently and was not contingent upon any external financial endorsements or grants.

REFERENCES

Al-Harthy, M., Begg, S., Bratvold, R. B. (2007). Copulas: A new technique to model dependence in petroleum decision making. *Journal of Petroleum Science and Engineering* 57, 1, 195-208.

Beck, J. V., Blackwell, B., & St Clair Jr, C. R. (1985). *Inverse Heat Conduction: Ill-Posed Problems*. New York: A Wiley-Interscience.

Desoutter, G., Cuenot, B., Habchi, C., Poinsot, T. (2005). The interaction of a premixed flame with a liquid fuel film on a wall. *Proceeding Combustion Institute* 30(1), 259-366.

Drake, M.C., Fansler, T.D., Solomon, A.S., Szekely, G.A. (2003). *Piston fuel films as a source of smoke and hydrocarbon emissions from a wall-controlled spark-ignited direct-injection engine* (Technical report No. 2003-01-0547). *SAE Technology Paper*.

Güralp, O.A. (2008). *The effect of combustion chamber deposits on heat transfer and combustion in a homogeneous charge compression ignition engine*. [Doctoral dissertation, Michigan University].

Güralp, O., Hoffman, M., Assanis, D.N., Filipi, Z., Kuo, T.W., Najt, P., Rask, R. (2009). *Thermal characterization of combustion chamber deposits on the HCCI Engine piston and cylinder head using instantaneous temperature measurements* (Technical report No. 2009-01-0668). SAE Technology Paper.

Han, Z., Yi, J., Trigui, N. (2002). *Stratified mixture formation and piston surface wetting in a DISI engine* (Technical report No. 2002-01-2655). SAE Technology Paper.

Hensel, S., Sarikoc, F., Schumann, F., Kubach, H., Velji, A., Spicher, U. (2009). A New model to describe the heat transfer in HCCI gasoline engines. *SAE International journal*: *Engines* 2, 1, 33–47.

Hoffman, M.A., Filipi, Z. (2015). *The influence of directly injected gasoline and porosity fraction on the thermal properties of HCCI combustion chamber deposits* (Technical report No. 2015-24-2449). SAE Technology Paper.

Jiao, Q., Reitz, R.D. (2014). Modeling soot emissions from wall films in a direct-injection spark-ignition engine. *International Journal of Engine Research* 16(8), 994–1013.

Kalghatgi, G.T. (1995). *Combustion chamber deposits in spark-ignition engines: a literature review* (Technical report No. 952443). SAE Technology Paper.

Kalghatgi, G.T., McDonald, C.R., Hopwood, A.B. (1995). *An experimental study of combustion chamber deposits and their effects in a spark-ignition engine*. (Technical report No. 950680). SAE Technology Paper.

Köpple, F., Seboldt, D., Jochmann, P., Hettinger, A., Kufferath, A., Bargende, M. (2014). Experimental investigation of fuel impingement and spray-cooling on the piston of a GDI engine via instantaneous surface temperature measurements. *SAE International Journal: Engines* 7, 3, 1178–1194.

Kubicki, M., Watson, H.C., Williams, J., Stryker, P.C. (2007). *Spatial and temporal temperature distributions in a spark ignition engine piston at WOT* (Technical report No. 4271). SAE Technology Paper.

LaVigne, P.A., Anderson, C.L., and Prakash, C. (1986). *Unsteady Heat Transfer and Fluid Flow in Porous Combustion Chamber Deposits* (Technical report No. 860241). SAE Technology Paper.

Litovsky E. Y., Shapiro M. (1992). Gas pressure and temperature dependences of thermal conductivity of porous ceramic material: part 1, refractories and ceramics with porosity below 30%. *Journal of American Ceramic Society* 75, 12, 3425–3439.

Liu, Y. C., Guessous, L., Sangeorzan, B. P. and Alkidas, A. C. (2015). Laboratory Experimental on Oil-Jet Cooling of Internal Combustion Engine Pistons: Area-Average Correlation of Oil-Jet Impingement Heat Transfer. *Journal of Energy Engineering* 141, 2, 1-10.

Liu, X.F., Wanga Y., and Liu W.H. (2017). Finite Element Analysis of Thermo-mechanical Conditions Inside the Piston of a Diesel Engine. *Journal of Applied Thermal Engineering* 119, 312-318.

Martin, G. G. (2004). Failure of Stationary Pump Engine Piston. *Journal of Failure Analysis and Prevention* 4, 1, 37–39.

Nakic. D. J., Dennis N. Assanis and Robert A. W. (1994). Effect of Elevated Piston Temperature on Combustion Chamber Deposit Growth. *Journal of Engines* 13, 1454-1466.

Noori, A.R., Rashidi, M. (2007). Computational fluid dynamics study of heat transfer in a spark-ignition engine combustion chamber. *Journal of Heat Transfer* 129, 5, 609- 616.

O'Rourke, P.J., Amsden, A.A. (1996). *A particle numerical model for wall film dynamics in port-injected engines* (Technical report N. 961961). SAE Technology Paper.

O'Rourke, P.J., Amsden, A.A. (2000). *A spray/wall interaction submodel for the KIVA-3 wall film model* (Technical report N. 0271). SAE Technology Paper.

Pedraza, D. and Klemens, P. (1993). Effective polycrystalline graphite. *Journal of Carbon* 31, 6, 951–956.

Pinto da Costa, J.M.C. (2010). *Structural characterization of carbonaceous engine deposits*. [Doctoral dissertation, The University of Edinburgh].

Szelagowski, H., Arvanitidis, I., and Seetharaman, S. (1999). Effective thermal conductivity of porous strontium oxide and strontium carbonate samples. *Journal of Applied Physics* 85, 1, 193–198.

X. Zhang et al. (2015). Investigating the microstructures of piston carbon deposits in a large-scale marine diesel engine using synchrotron X-ray microtomography, *Journal of Fuel* 142, 173-179.

Weidenlener, A., Pfeil, J., Kubach, H., Koch, T., Forooghi, P., Frohnapfel, B., & Magagnato, F. (2018). The influence of operating conditions on combustion chamber deposit surface structure, deposit thickness, and thermal properties. *Journal of Automotive and Engine Technology* 3, 111-127.